MONTE-CARLO SIMULATIONS OF TIME-RESOLVED, OPTICAL READOUT DETECTOR for PULSED, FAST-NEUTRON TRANSMISSION SPECTROSCOPY (PFNTS)

Ilan Mor[a*] , **David Vartsky**[a], **I. Mardor**[a], **M. B. Goldberg**[a], **D. Bar**[a], **G. Feldman**[a],
V. Dangendorf[b],   **A. Breskin**[c],   **R. Chechik**[c]

[a]*Soreq NRC, Yavne, Israel,* [b]*Physikalisch-Technische Bundesanstalt (PTB), Braunschweig, Germany,*
[c]*Weizmann Institute of Science, Rehovot, Israel*

Over the past two years, we have developed and tested an efficient, large-area, sub-mm spatial-resolution, fast-neutron imaging system with time-of-flight spectroscopic capability. The detector is based on a 30 mm thick scintillating fiber screen viewed by a time-gated optical readout, described in another contribution to this conference.

In order to analyze key parameters affecting detector performance, Monte-Carlo simulations using the GEANT 3.21 code were performed. To characterize the intrinsic spatial resolution of the scintillating fiber screen, a neutron transmission image of a steel mask containing a series of slits with various widths, pitch and thicknesses was simulated. The point spread function of the scintillating fiber screen was determined by exposure to an infinitesimally narrow neutron beam, incident perpendicular to the surface, calculating the spatial distribution of the energy deposited by the protons in the screen fibers. The energy distribution of the (n,p) protons produced in the screen and the amount of scintillation light subsequently created were also calculated. All the above simulations were performed for 3 neutron energies (2, 7.5 and 14 MeV).

For the detector tests performed at the PTB cyclotron, the neutron beam-line geometry was simulated as accurately as possible, in order to calculate the contribution of neutron scatter as well as gamma rays and to enable a comparison with the experimental results.

---

[*] Ilan Mor   ilmor@soreq.gov.il

1. Introduction

TRION (Time Resolved Integrative Optical (readout for) Neutrons) is a novel, fast-neutron imaging device based on time-gated optical readout. The concept was first proposed by Dangendorf et al. [1] of the PTB Institute, Germany and subsequently developed at Soreq NRC in close collaboration with the PTB group.

The detector is designed to detect fast-neutron pulses produced, for example, in the $^9Be(d,n)$ reaction using a pulsed (~1 ns bursts, 1-2 MHz repetition rate) deuteron beam. As illustrated in another contribution to these proceedings [2], these fast-neutron pulses impinge on a scintillator screen (polystyrene) causing the emission of light from the screen via knock-on protons. The light is reflected by a front-coated bending mirror (98% reflectivity, positioned at an angle of 45° relative to the neutron beam direction) towards a large aperture 120 mm F#0.95 lens. The light is amplified by a ns-gated image intensifier and transmitted by an optical tandem assembly comprising a 200 mm lens (F#=2.8) and a 50 mm lens (F#=1.2) coupled to a cooled CCD camera.

The gated image intensifier acts as a fast electronic shutter for the CCD camera. By selecting the gate time relative to the neutron beam pulse, it is possible to define a time window (gate width) that corresponds to a preselected neutron energy bin. In a typical pulsed fast-neutron beam, the burst rate is of the order of 2 MHz. Within a time period of 500 ns, depending on neutron-source to detector distance, the system should integrate neutrons into an image in a well defined time window (typical gate width is 2-10 ns).

Thus, the detector is based on an integrative (as opposed to single-event counting) optical technique, which permits neutron energy-resolved imaging via time-gated optical readout. This mode of operation permits loss-free operation at very high neutron-flux intensities.

The TRION neutron imaging system can be regarded as a stroboscopic photography of neutrons arriving at the detector on a few-ns time scale. Although stroboscopic time-resolved optical imaging techniques have previously been used to determine various physical properties, no time-resolved neutron imaging has yet been performed.

1.1 GEANT simulations

The scintillator mounted in the TRION system is a polystyrene fiber scintillator screen. The reason for using scintillating optical fibers, rather than a plain scintillator slab, is to maintain spatial resolution independent of screen thickness.

In order to determine light yield, spatial resolution and dependence of Contrast[*] Transfer Function (CTF) on neutron energy, GEANT simulations were performed.

The CTF [3] represents the response of an imaging system to a constant square-wave input in terms of spatial frequency and is used to quantify the imaging system's ability to transfer contrast from an object to an image at various resolution levels or spatial frequencies. As the

---

[*] Image contrast = (max. brightness – min. brightness) / (max. brightness + min. brightness)

spatial frequency increases, the observable image contrast decreases. It is this loss of contrast at higher spatial frequencies that characterizes the performance of the imaging device.

In order to calculate the CTF, an image profile (see fig. 1) depicting the system's response to a constant square-wave input mask (such as the one seen in fig. 5) is analyzed.

The CTF at a certain spatial frequency ω is calculated using the maximum (I_{max}) and minimum (I_{min}) transmission values, also seen in fig. 1:
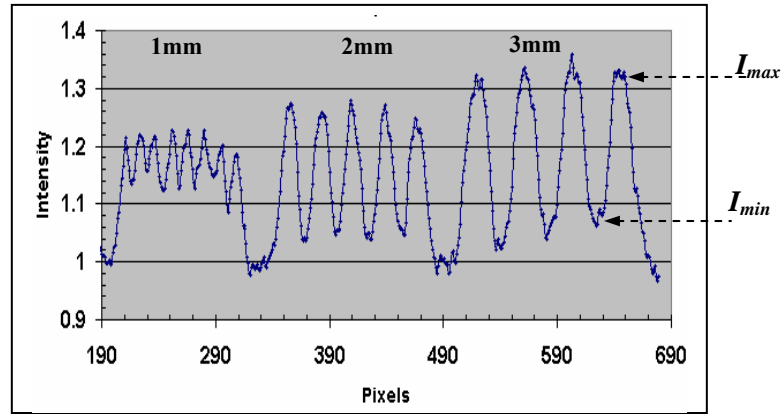
Fig. 1   Image profile containing three different spatial frequencies

$$Modulation\,(\omega) \;\; = \frac{I_{\max}(\omega) - I_{\min}(\omega)}{I_{\max}(\omega) + I_{\min}(\omega)} \qquad\qquad (1)$$

$$CTF(\omega) = \frac{Modulation(\omega)}{Modulation(\omega_o)} \qquad\qquad (2)$$

The convention employed is that each modulation ($modulation(\omega)$) is normalized by the modulation of the zero spatial frequency ($modulation(\omega_o)$, a step function) which represents the best achievable contrast.

A common reference unit for spatial frequency is the number of line pairs per millimeter (lp/mm). For example, a continuous series of black and white line pairs measuring 0.5 mm per pair would repeat twice every millimeter, thus having a corresponding spatial frequency of 2 lp/mm.

The spectra measured by TRION may contain other events than fast neutrons emitted directly from the target. These are primarily due to neutrons scattered by the collimators, as well as gamma-rays produced in the collimation system by inelastic neutron scattering and neutron capture. In order to determine their contribution and time behavior, the entire neutron conversion process in the scintillator was simulated using the GEANT 3.21 code [4]

2.1 Energy deposition and light creation by protons

In order to determine the distribution of energy deposited in the fibers and the amount of light created by the neutrons, we have performed a GEANT simulation of the energy deposited by protons in a 0.5×0.5 mm^2 pixel of a fiber screen $200 \times 200 \times 20$ mm^3 in dimensions.

In this simulation, the fiber screen was irradiated uniformly by neutrons incident normal to its face. Fig. 2 shows the distribution of the energy deposited by the protons in the fiber. The average proton energy is 0.78, 2.44 and 3.22 MeV for the 2, 7.5 and 14 MeV neutrons, respectively.

As can be observed the distribution approximates the flat shape only for the low energy neutrons, for which the corresponding knock-on proton deposits most of its energy in the fiber. As the neutron energy increases the proton can escape the fiber in which it was created and the energy is distributed in more than one fiber.

Using the known entrance and exit energies of each proton in the fiber we have also calculated the average number of light photons created in the fiber by the incident neutrons, using the non-linear proton-energy to-light conversion relation for a plastic scintillator (see fig. 3) [5].

The simulation yielded average amounts of light photons created in a single fiber of 2600, 10600 and 17400 for 2, 7.5 and 14 MeV neutrons, respectively.
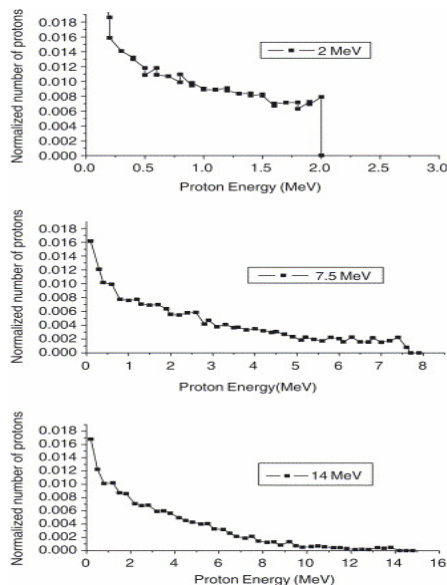
Fig. 2   Spectra of energy deposited by protons in 0.5×0.5-mm² fibers for 2 (top),   7.5 (middle) and   14 MeV (bottom) neutrons. The number of protons was normalized to the number of incident neutrons/pixel
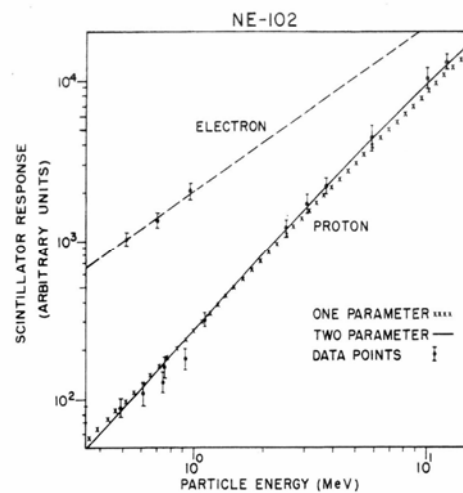
Fig. 3   Scintillation light yield for a common plastic scintillator (NE 102) when excited by electrons and protons [5]

2.2 Spatial resolution

The spatial resolution of the scintillating fiber screen was determined using GEANT. In these simulations the Point Spread Function (PSF) was determined by exposure of the fiber screen to an infinitesimally narrow neutron beam, incident normal to its surface. Fiber dimensions were 0.5×0.5×30 mm³. The amount of light created in the irradiated fiber and in the fibers adjacent to it was determined. Fig. 4 shows the PSF for the fiber screen, simulated for neutrons of 3 different energies: 2, 7.5 and 14 MeV. Table 1 lists FWHM and FWTM (Full Width Tenth Maximum) derived from the PSF simulations.
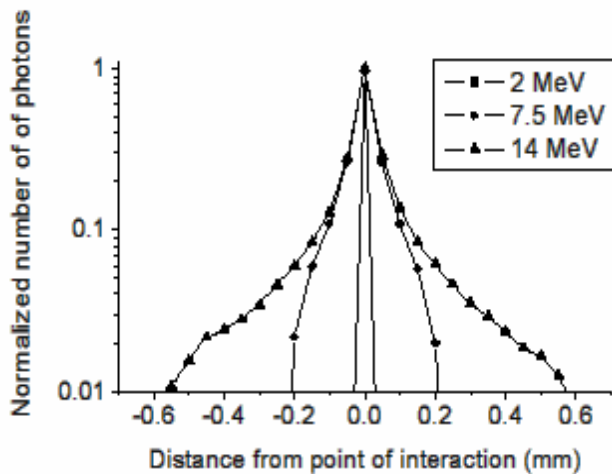
Table 1   FWHM and FWTM (Full Width Tenth Maximum) of TRION's PSF

Neutron energy (MeV)	FWHM (µm)	FWTM (µm)
2.0	~60	80
7.5	90	200
14.0	100	300

Fig. 4   Point Spread Function (PSF) of the fiber screen

As expected, the PSF broadens as neutron energy increases. Neutrons of higher energies cause the emission of more energetic knock-on protons, which translates to larger range within the screen.

2.3 CTF variation with neutron energy

The spatial resolution of a scintillating fiber screen is affected by the fiber cross-sectional dimensions, range of the knock-on proton generated by the incident neutron, multiple scattering of neutrons within the screen and light cross-talk between fibers.

Fiber diameter determines the inherent spatial resolution achievable with the fiber scintillator screen. Furthermore, the radially projected range (perpendicular to the neutron flight direction) of the recoil proton is also of importance. A recoil proton may cover a distance of several hundred microns (a ~3.75 MeV proton may travel 203 µm within polystyrene [6]) before coming to rest within the scintillator. The average proton energy which translates to radially projected range within the scintillator is determined by the neutron energy. Thus, the achievable spatial resolution is also influenced by the neutron energy.

In order to determine the variation of spatial resolution with neutron energy, a radiographic image of the steel mask shown in fig. 5 was simulated. The fiber size was 500×500 µm^2 and the distance between the Be target and the fiber screen was 12 m. The deuteron beam diameter on the target was 5 mm and the steel mask was positioned at a distance of 15 cm from the screen, as in the actual experiment.

The GEANT simulation calculated the total amount of energy deposited in a fiber by protons created directly in the fiber and by protons entering the fiber from the surrounding area. In addition, the simulation calculated the amount of light photons

Fig. 5   Steel mask

5
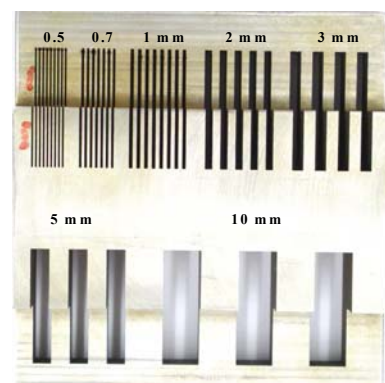
generated in a fiber by each proton, taking into account the non-linear behaviour of the light-energy relation for protons.

Fig. 6 shows a profile taken over the high frequency portion of the steel mask with 2 MeV neutrons. Similar profiles were created for each of the above neutron energies.

The CTF was calculated for each of the simulated profiles, as shown in fig. 7.
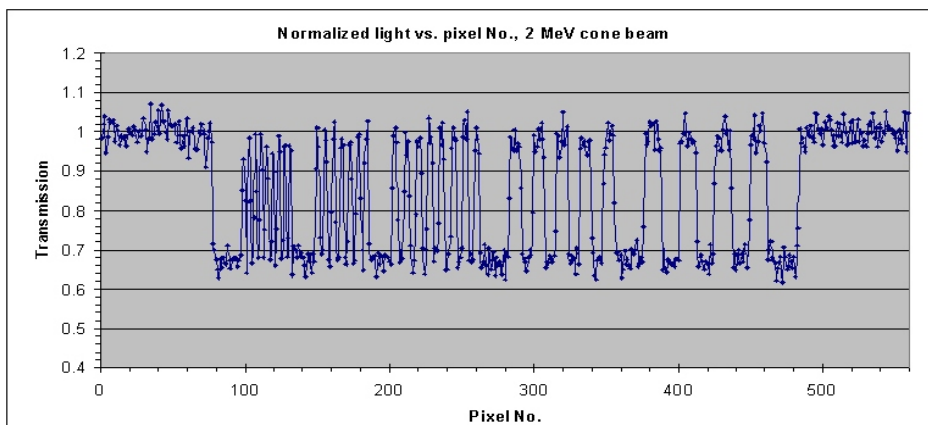
Fig. 6 Profile taken over the high frequency portion of the steel mask, simulated for 2 MeV neutrons
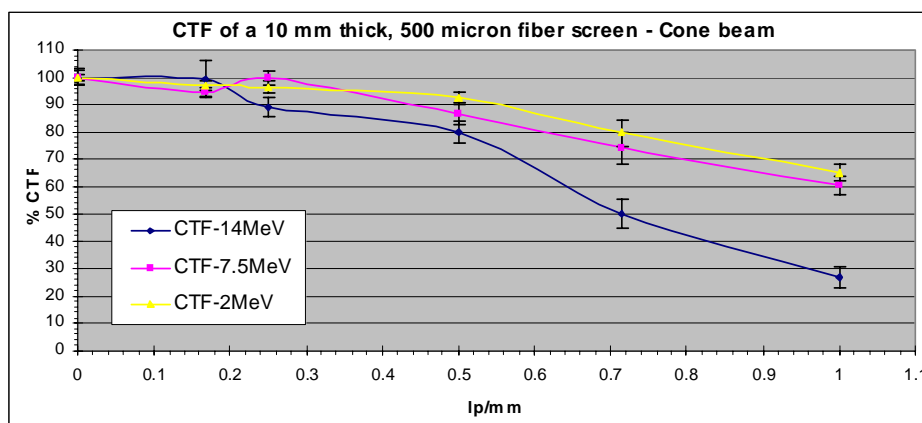
Fig. 7 Intrinsic *CTF* of 10 mm thick scintillating fiber screen (500 μm fiber dimension), simulated for 2, 7.5 and 14 MeV neutrons

As can be observed the CTF decreases with spatial frequency. CTFs resulting from 2 and 7.5 MeV neutrons are only minimally different since the maximal ranges of 1 MeV and 3.75 MeV protons (average proton energy) within polystyrene are 22 and 203 μm, respectively [6]. These are smaller than the size of a 500 μm fiber. In contrast, for 14 MeV neutrons, the range of a 7 MeV proton is 608 μm [6], causing a significant deterioration of CTF at frequencies higher than 0.5 lp/mm.

3. Simulation of beam transport

The spectrum of neutrons arriving at the detector may contain other events than fast neutrons emitted directly from the target. These are primarily due to neutrons scattered by the

6

collimators, as well as gamma-rays produced in the collimation system by inelastic neutron scattering and neutron capture. In order to determine their contribution and time behavior, the experimental setup (shown in fig. 8) was simulated.
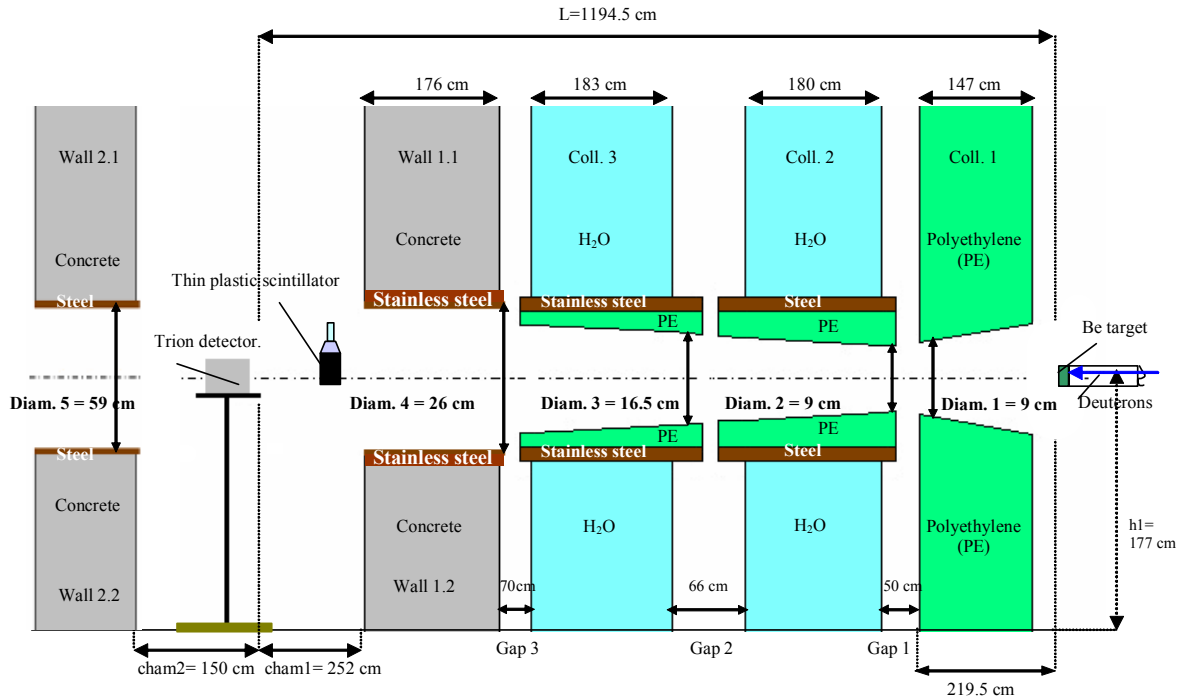
Fig. 8 Cross-section schematic diagram of the PTB experimental setup (not to scale) for 0° beam-line

All simulations related to a cone-beam of **12.16** MeV mono-energetic neutrons emitted from a point source, air humidity of 55%, neutron energy cutoff of 12 keV and beam opening angle of 9° (as illustrated in fig. 9).

3.1 Influence of scattered neutrons

Fig. 10 displays the simulated TOF spectrum of the scattered neutrons entering the detector. The ratio of the scattered neutrons to the direct ones (all neutrons which enter the detector) is 2.5×10^{-3}. This small ratio is clearly a consequence of the efficient PTB neutron collimation & anti-scattering system, implying that neutrons scattered by the collimation system will not constitute a significant source of image degradation.
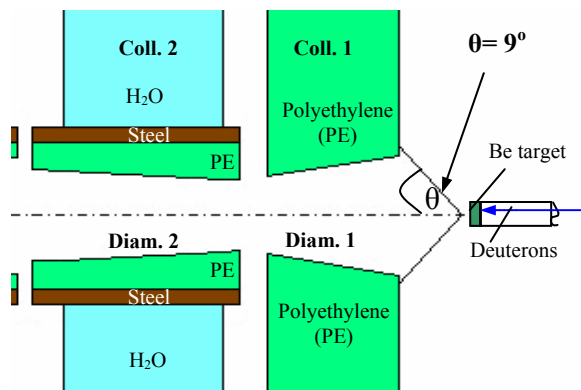
Fig. 9 A section of the collimation system with illustration of neutron beam opening angle of 9°

7
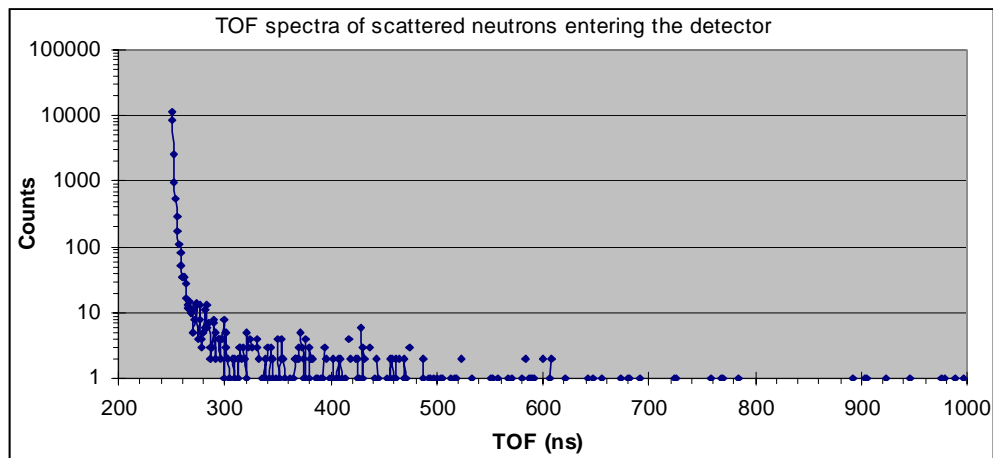
Fig. 10   TOF spectrum of scattered neutrons entering the detector. TOF of unscattered neutrons is 249.944 ns

3.2 Gamma ray background

The number of gamma photons entering the detector was also simulated (see fig. 11). The ratio of gamma photons to the number of direct neutrons (all entering the detector) is 4.7×10^{-3}. This rather low ratio does not take into account gamma rays produced by neutrons of energies lower than 12 keV (due to the fact that GEANT 3.21 has a cutoff limit of 10 keV).
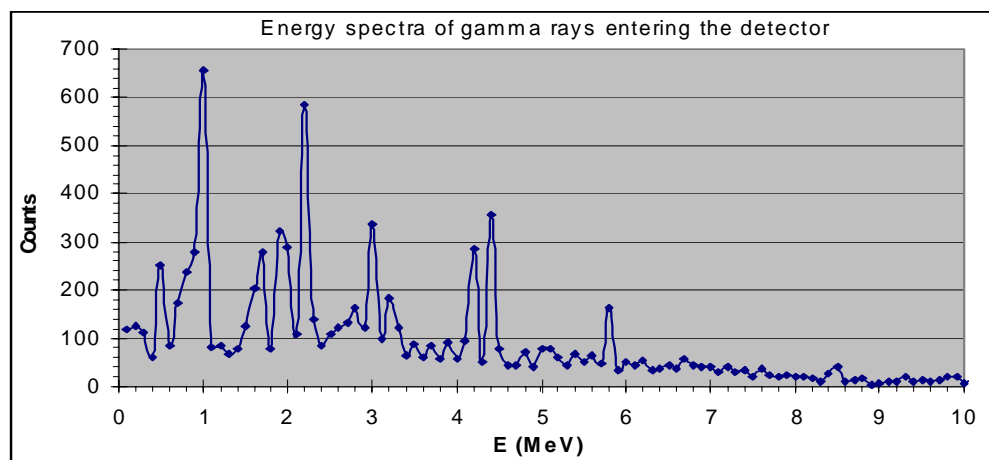
Fig. 11   Energy spectrum of gamma rays entering the detector

From these calculations, it can be concluded that the number of neutrons and gamma-rays which contribute to the background is negligible.

3.3 Summary

The performance of a neutron converter composed of scintillating polystyrene fibers, employed in a fast-neutron imaging detector, was analyzed using Monte Carlo methods. At low neutron energies, where the radially projected range of the recoil protons is much smaller than

8

the fiber dimensions, spatial resolution is independent of neutron energy and is determined by fiber dimensions.

At higher neutron energies, the achievable spatial resolution deteriorates due to the higher radially projected range of the recoil protons. Hence, using fibers of very small radial dimensions will not significantly improve spatial resolution. Instead, out of cost considerations, one should optimize fiber radial dimensions according to the neutron spectrum characteristic of the respective application.

The background level due to gamma rays and scattered neutrons at the PTB cyclotron beam-line is rather low and can be neglected.

Acknowledgements

References

[1] V. Dangendorf, Kersten C., Laczko G., Jaguztky O., Spillman U., *Fast Neutron Resonance Radiography in a Pulsed Neutron Beam*, Contribution to 7th World Conference on Neutron Radiography, Rome, Sept 2002, http://arxiv.org/abs/nucl-ex/0301001

[2] D. Vartsky, *Prospects of fast-neutron resonance radiography and requirements for instrumentation*, in proceedings of the FNDA2006 workshop

[3] Logory L. M., Farley D. R., Conder A. D., Belli E. A., Bell P. M., miller P.L., *Characterization of an X-ray framing camera utilizing a charge coupled device or film as recording media*, Review of scientific instruments 69(1998)

[4] GEANT 3.21, *detector description and simulation tool*, CERN program library long writeup.

[5] G. F. Knoll, *Radiation Detection and Measurement*, John Wiley and Sons

[6] J. F. Janni, *Proton range-energy tables: 1 keV-10 GeV*, Atomic data and Nuclear data tables Vol. 27 (1982) 304-305